Thomson Scattering from High-Z Laser-Produced Plasmas

S. H. Glenzer,[1] W. Rozmus,[2,*] B. J. MacGowan,[1] K. G. Estabrook,[1] J. D. De Groot,[1,3] G. B. Zimmerman,[1]
H. A. Baldis,[2] J. A. Harte,[1] R. W. Lee,[1] E. A. Williams,[1] and B. G. Wilson[1]
[1]*L-399, Lawrence Livermore National Laboratory, University of California, P.O. Box 808, Livermore, California 94551*
[2]*Institute for Lasers Science Applications, University of California, Livermore, California 94550*
[3]*Department of Applied Science and Plasma Research Group, University of California, Davis, California 95616*
(Received 30 September 1998)

We present the first simultaneous observations of ion acoustic and electron plasma waves in laser-produced dense plasmas with Thomson scattering. In addition to measuring the standard plasma parameters, electron temperature and density, this novel experimental technique is shown to be a sensitive method for temporally and spatially resolved measurements of the averaged ionization stage of the plasma. Experiments with highly ionized gold plasmas clearly show that the inclusion of dielectronic recombination in radiation-hydrodynamic modeling is critically important to model cooling plasmas. [S0031-9007(98)08073-9]

PACS numbers: 52.70.Kz, 52.35.Fp, 52.40.Nk, 52.50.Jm

Highly ionized plasmas have been extensively produced in many laboratories to study radiative properties of hot dense matter [1,2] and for a variety of applications related to inertial confinement fusion (ICF) research, lithography, microscopy, laboratory astrophysics, or x-ray lasers. The averaged ionization stage $\bar{Z}$ of these plasmas is a particularly important parameter because it determines basic physical quantities such as collision rates and acoustic velocities and is therefore a critical parameter for the x-ray production (e.g., Ref. [3]).

In indirect-drive ICF research [4], high-Z hohlraums are used as radiation enclosures to convert optical laser light into x rays which drive the implosion of the fusion capsule. In this scheme, the coupling of high-energy, high-power lasers with matter and its conversion into x rays depends on inverse bremsstrahlung absorption and on laser scattering losses such as stimulated Brillouin (SBS) and stimulated Raman scattering [5]. These processes are known to be sensitive to the charge state $\bar{Z}$ of the plasma [6,7]. In particular, the damping of ion acoustic waves driven by SBS depends on the *local* value of $\bar{Z}$ in the dense, highly ionized gold plasma close to the hohlraum walls [8]. Thus it is important to develop an accurate diagnostic for local measurements of $\bar{Z}$ and to test our understanding of this parameter by comparing accurate experiments with radiation-hydrodynamic calculations.

In this Letter, we present the first simultaneous observations of ion acoustic and electron plasma wave fluctuation spectra in a dense plasma using Thomson scattering (TS) (e.g., Refs. [9,10]). This experiment gives accurate spatially and temporally resolved information on plasma parameters; in particular, we present the first measurements of the ionization stage $\bar{Z}$ of a high-Z plasma using incoherent TS. In this experiment, we scatter from electron plasma waves that are strongly Landau damped allowing a direct measurement of the electron density n_e and temperature T_e of the plasma. The frequency of the simultaneously observed ion acoustic waves, which is proportional to $\sqrt{\bar{Z}T_e}$, is then used to obtain an accurate value for the charge number $\bar{Z}$. The analysis of the Thomson scattered radiation has been performed with a generalized theory of the TS cross section, which includes the effect of gradients in the plasma, collisions, and non-Maxwellian velocity distributions. We find that *local* electron temperatures, T_e, electron densities, n_e, and the ionization stage, $\bar{Z}$, of the plasma can be measured with uncertainties of $<20\%$. This degree of accuracy allows us to test various atomic physics models. The present study shows for the first time that radiation-hydrodynamic modeling using the code LASNEX with an average atom model (XSN) [11] significantly overestimates $\bar{Z}$ in a recombining plasma. Models with more detailed atomic physics spectra and opacities [detailed configuration accounting (DCA)] [12] show an improved description of the plasma conditions due to the inclusion of dielectronic recombination.

The experiments were performed with the 30 kJ Nova laser facility at the Lawrence Livermore National Laboratory [13]. It is a Nd:glass laser operating at 1.053 μm (1ω) which can be frequency converted to 2ω or 3ω. A small part of the laser beam was recently separated out and frequency quadrupled providing an independent 4ω-TS probe laser [14]. A 3ω- ($\lambda = 351$ nm) heater beam was smoothed with a kinoform phase plate to produce the plasma by irradiating a flat gold disk at an angle of 64° to the disk normal. A 1.5-ns-long flat-topped laser pulse with 100-ps rising and falling edges was used with a total energy of 3.8 kJ. The focal spot size was measured by two-dimensional plasma x-ray imaging to be 400×600 μm^2 indicating a laser intensity of $I = 10^{15}$ W cm^{-2} on target.

4ω TS was performed at various distances from the surface of the Au disk including the high density plasma regions close to the disk surface that cannot be diagnosed

with a 2ω laser. The 4ω probe laser was operated at an energy of 50 J in a 1.5-ns square pulse. These measurements are important to characterize the temperature and flow gradients [15,16] of the plasma and to validate the Thomson scattering cross section applied below. Figure 1(a) shows temporally resolved streak data at 4ω for various positions in the plasma corona schematically shown in Fig. 1(b). The probe laser was parallel to the disk and focused to ~ 100 μm diameter giving a cylindrical scattering volume. Its length is determined by the imaging optics ($f/10$) and is 70 μm for the 1.5 magnification and 100-μm detector slit size. The scattering angle was chosen to be $\theta = 90°$ for the 4ω measurements and a 1-m spectrometer with an optical S-20 streak camera was employed to detect the TS spectra with a temporal resolution of 30 ps and a wavelength resolution of 0.05 nm. The total time interval during which the streak camera detects data is 3 ns. This duration is small compared to the time the 4ω laser light needs to travel from the Nova target chamber walls to the detector resulting in very small stray light levels in the present experiments.

The scattering geometry [Fig. 1(b)], probe laser wavelengths, and the plasma parameters result in collective TS (e.g., Refs. [17–19]) from fluctuations characterized by wave numbers, k, such that $\alpha = 1/k\lambda_D = 1 - 2$, where

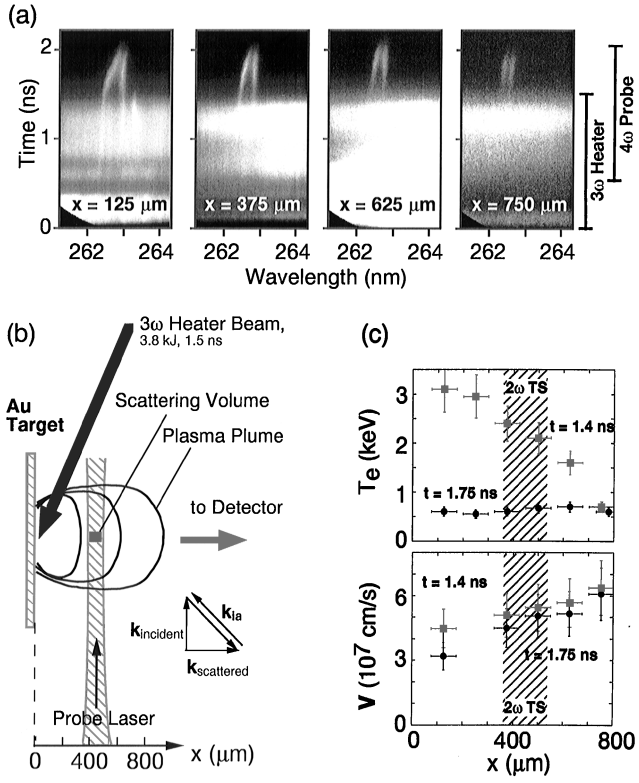

FIG. 1. 4ω Thomson scattering data (a) together with a schematic of the experiment (b) and the measured temperature T_e and flow V gradients (c). The shaded region indicates the plasma region diagnosed by the 2ω probe. At late times, $t > 1.5$ ns, the 2ω probe will elevate T_e.

λ_D is the electron Debye length. In this regime, the scattered light spectrum consists of the ion and the electron features. They correspond to scattering resonances at the ion acoustic wave (iaw) and at the electron plasma wave (epw) frequencies shifted from the incident probe laser frequency on either side on the frequency scale. In Fig. 1(a) we clearly observe two ion acoustic scattering resonances for 0.8 ns $< t <$ 2 ns. The frequency separation of the two peaks is twice the ion acoustic frequency, ω_{ia},

$$\left(\frac{\omega_{ia}}{k_{ia}}\right)^2 \simeq \frac{T_e}{M}\left(\frac{\bar{Z}}{1 + k_{ia}^2\lambda_D^2} + \Gamma_i\frac{T_i}{T_e}\right) \approx \frac{T_e}{M}\left(\frac{\bar{Z}}{1 + k_{ia}^2\lambda_D^2}\right), \quad (1)$$

where M is the ion mass, T_i is the ion temperature, Γ_i is the specific heat ratio, and the scattering vector k_{ia} is given by the triangle relation [9] shown in Fig. 1(b).

Equation (1) illustrates that T_e can be deduced from the frequency separation ω_{ia} if $\bar{Z}$ is known independently or vice versa. Employing a high-energy 2ω probe, we have measured T_e from the damping of the epw resonance described below so that we could subsequently deduce $\bar{Z}$ from the simultaneously measured ion acoustic waves. Since it is found that $\bar{Z}$ varies slowly in space, we can use the data shown in Fig. 1(a) to illustrate the corona temperature conditions. While the heater beam is on and deposits its energy into the disk ($t =$ 1.4 ns), a temperature gradient with scale length of $L_T =$ 800–1800 μm exists. After the heater beam has turned off ($t > 1.5$ ns) the corona becomes rather isothermal [$L_T > 3000$ μm; Fig. 1(c)]. In addition, we find due to the supersonic expansion of the corona that the TS spectra are Doppler shifted to the blue. This can easily be seen in the spectrum measured at $x = 125$ μm [Fig. 1(a)] where the stray light from the 4ω probe laser is clearly observable at $\lambda_i = 263.3$ nm. We find a flow gradient scale length of $L_V = 400$–800 μm [Fig. 1(c)].

To simultaneously measure the iaw and the epw features of the TS spectrum it was necessary to apply a high-energy 2ω probe laser. The use of a probe laser energy of ~ 500 J at 2ω in a 4-ns square pulse was made necessary by high background levels in the ultraviolet spectral range due to bremsstrahlung, stray light from the heater beam, and the fact that the electron feature has about an order of magnitude smaller amplitude than the ion feature. Similar to the 4ω TS measurements, the 2ω probe laser was parallel to the disk. The probe beam was focused to 170 μm diameter at a distance of $x = 450$ μm. In addition to the measurements of the ion feature, we observed the electron feature in the wavelength range of 500–800 nm using a beam splitter and a 1/4-m spectrometer with a wavelength resolution of 1.3 nm. In this way both detectors observed essentially the same volume in the plasma. A second streak camera (S-1) was employed to record the electron feature with a temporal resolution

of 150 ps. To avoid saturation of this detector by the ion feature we used an optical filter suppressing radiation with $\lambda < 550$ nm.

Figure 2 shows experimental 2ω TS spectra of the ion feature (a) and of the electron feature (b) together with a theoretical fit using the following expression for the scattered power, P_s, into a solid angle $d\Omega$ per frequency range $d\omega$ [20],

$$\frac{dP_s}{d\Omega\, d\omega} = \frac{\hat{\eta}_1 \cdot \hat{\eta}_2}{2\pi} r_0^2 \int dx\, S(\mathbf{k}, \omega; x) n_e(x) \times \int d^2 r_\perp \frac{c E_0^2(\mathbf{r})}{8\pi}, \quad (2)$$

where $\hat{\eta}_i$ $(i = 1, 2)$ are polarization vectors defining the directions of the Thomson probe electric field E_0 and of the scattered light detection; $r_0 = e^2/m_e c^2$. The dynamical form factor describing fluctuations at wave number $\mathbf{k}$ and frequency ω, $S(\mathbf{k}, \omega; x)$, has been calculated locally to take into account the spatial variations of n_e, T_e, and V along the direction x, normal to the disk. It further includes collisional effects [21,22], super-Gaussian electron velocity distribution functions [23,24], and Spitzer-Härm [25] electron transport.

Figure 2(b) shows the electron feature at various times showing a heavily damped epw resonance with a wavelength shift that decreases as the heater beam turns off. The wavelength shift is approximated by the Bohm-Gross dispersion relation $\omega^2 = \omega_p^2 + 3k_{\mathrm{epw}}^2 T_e/m_e$, where ω_p is the plasma frequency. This relation indicates that the electron density of the plasma can be obtained with high accuracy ($\sim$15%) because we can precisely determine T_e by fitting the overall shape of the epw resonance in this strongly damped regime. For example, the fit at $t = 1.4$ ns gives $T_e = 2.0$ keV and $n_e = 2.1 \times 10^{20}$ cm^{-3} including gradients as measured with the 4ω probe. Without gradients the width of the peak at 735 nm is smaller than observed. It turns out that the fit is fairly robust.

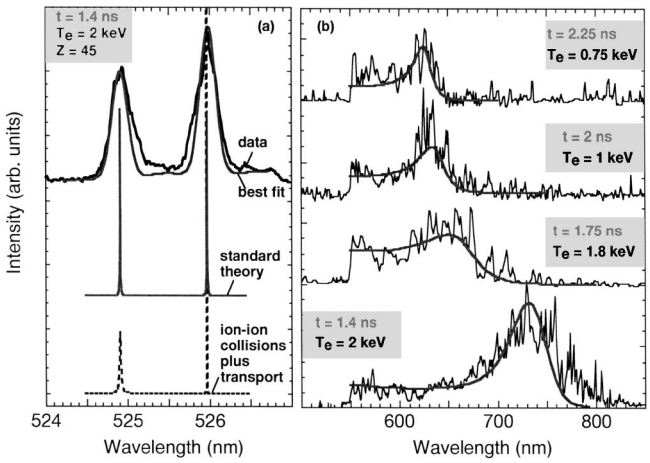

FIG. 2. Measured ion (a) and electron (b) feature of the Thomson scattering spectrum along with theoretical fits.

Increasing Landau damping by increasing T_e results in a broader electron feature but also shifts the resonance to larger wavelengths (Bohm-Gross relation). To compensate for this shift, one has to assume a smaller electron density which in turn reduces electron Landau damping, and this fit does not converge.

Since electron Landau damping is sensitive to the electron velocity distribution function, the experimental data also give information about the possible presence of non-Maxwellian distributions in the plasma. Predictions from Fokker-Planck calculations [26] result in a super-Gaussian distribution, $f \sim \exp(-v^m)$, with an exponent in the range of $m = 3.5$–4 for the averaged intensity of the 2ω probe laser. However, we find that at $t = 1.4$ ns the electron feature is fitted best by a Maxwellian distribution ($m = 2$) while, e.g., $m = 3$ results in a resonance that is too narrow, not consistent with the measured gradients in the plasma. The predictions likely overestimate m because in the present experiment, lateral electron transport out of the probe beam volume plays an important role which is not accounted for in the calculations. When the plasma cools, e.g., at $t = t_0 + 2$ ns, the experimental data can be fitted with a distribution with $m = 2.4 \pm 0.3$. This deviation from a Maxwellian appears to be insignificant as it introduces only a $\sim$5% correction to the parameters deduced from the TS spectra.

Using the parameters from the epw resonance shown in Fig. 2(b), we obtain $\bar{Z}$ of the plasma by fitting the simultaneously measured ion acoustic wave spectrum as shown in Fig. 2(a). This example shows the ion feature measured at $t = 1.4$ ns, a calculated form factor from the standard collisionless theory (e.g., Ref. [10]), theoretical results including ion-ion collisions and modification to the distribution function due to Spitzer-Härm thermal transport [21], and the final theoretical fit [Eq. (2)]. The ion acoustic peaks are significantly broadened due to the inhomogeneity of the plasma in the scattering volume. The measured temperature gradient implies a heat flux and a corresponding skewing of the distribution function. This results in different Landau damping of the two ion acoustic peaks but does not change their frequencies. Accounting for this asymmetry, the broadening from the instrument (0.05 nm) and the spatial gradients allow a fit of the entire spectrum. T_e is given by the electron feature with an error of about 15%, by varying the calculated spectra within the noise of the data. Therefore, we can deduce the averaged charge state $\bar{Z}$ from the ion feature with an error of 20%.

Figure 3 shows a compilation of the experimental data T_e, n_e, and $\bar{Z}$ together with two-dimensional simulations using the radiation-hydrodynamic code LASNEX [27] with two atomic physics packages. Both the calculations with an average atomic physics model (XSN) [11] and the calculations with detailed configuration accounting including $\sim$1000 levels [12] are in broad agreement with the measurements during the heater beam pulse up to 1.5 ns.

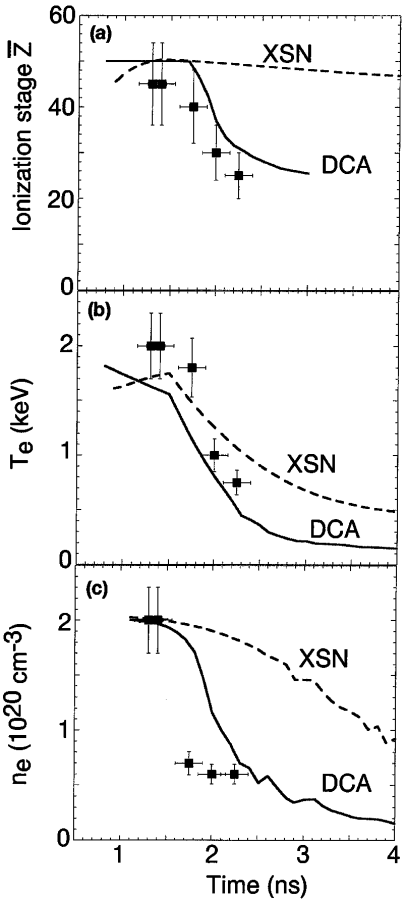

FIG. 3. Comparison of $\bar{Z}$ (a), T_e (b), and n_e (c) from Thomson scattering with two-dimensional hydrodynamic simulations using an averaged atomic physics model (XSN) and a detailed spectra and opacity model (DCA).

After the heater has turned off, we observe that the averaged atom model significantly overestimates the charge state $\bar{Z}$ of the plasma. On the other hand, the DCA model is in agreement with the experimental data. This improved description of the plasma conditions is due to dielectronic recombination. DCA calculations without dielectronic recombination show a slow decrease of the parameters more similar to the XSN model. To ensure that the modification of the schematic model to include dielectronic recombination is correct, we determine the steady state gold ionization balance using a Monte Carlo method [28] with a screened hydrogenic model. The results indicate that indeed the dielectronic recombination does change the ionization balance as predicted by DCA. As a consequence of dielectronic recombination the modeled electron density with DCA decreases on a time scale of 100–300 ps in excellent agreement with the experimental observations.

In summary, we have demonstrated that Thomson scattering is a novel experimental technique to measure T_e, n_e, and $\bar{Z}$ in dense plasmas with high spatial and temporal resolution. This unique data set has allowed us to demonstrate the importance of dielectronic recombination in cooling high-Z plasmas. These results provide a critical step in understanding the x-ray production and radiative properties of dense matter such as those encountered in ICF plasmas, where the late time x-ray drive is presently not well understood [29].

We thank the Nova crew for their efforts and D. Bailey, H. R. Griem, and L. J. Suter for discussions. This work was performed under the auspices of the U.S. Department of Energy by the Lawrence Livermore National Laboratory under Contract No. W-7405-ENG-48.

*On sabbatical from Department of Physics, University of Alberta, Edmonton, Alberta, Canada T6G2J1.

[1] R. W. Lee *et al.,* "Science on Lasers," Lawrence Livermore National Laboratory Report No. UCRL-ID-119170, 1994.
[2] F. J. Rogers and C. A. Iglesias, Science **203**, 50 (1994).
[3] P. Celliers and K. Eidmann, Phys. Rev. A **41**, 3270 (1990).
[4] J. D. Lindl, Phys. Plasmas **2**, 3933 (1995).
[5] W. L. Kruer, *The Physics of Laser Plasma Interactions* (Addison-Wesley, New York, 1988).
[6] R. K. Kirkwood *et al.,* Phys. Rev. Lett. **77**, 2706 (1996).
[7] J. C. Fernandez *et al.,* Phys. Rev. Lett. **77**, 2702 (1996).
[8] R. L. Berger (private communication).
[9] H.-J. Kunze, in *Plasma Diagnostics,* edited by W. Lochte-Holtgreven (North-Holland, Amsterdam, 1968), p. 550.
[10] J. Sheffield, *Plasma Scattering of Electromagnetic Radiation* (Academic, New York, 1975), and references therein.
[11] J. A. Harte *et al.,* "LASNEX-A 2-D Physics Code for Modeling ICF," LLNL Report No. UCRL-LR-105821-96-4, 1996.
[12] Y. T. Lee, J. Quant. Spectrosc. Radiat. Transfer **38**, 131 (1987).
[13] E. M. Campbell *et al.,* Laser Part. Beams **9**, 209 (1991).
[14] S. H. Glenzer *et al.,* Rev. Sci. Instrum. (to be published).
[15] J. S. Wark *et al.,* Phys. Rev. Lett. **72**, 1826 (1994).
[16] P. Young, Phys. Rev. Lett. **73**, 1939 (1994).
[17] H. A. Baldis *et al.,* Can. J. Phys. **64**, 961 (1986).
[18] A. A. Offenberger *et al.,* Phys Rev. Lett. **71**, 3983 (1993).
[19] C. Labaune *et al.,* Phys. Rev. Lett. **75**, 248 (1995).
[20] W. Rozmus *et al.* (to be published).
[21] J. F. Myatt *et al.,* Phys. Rev. E **57**, 3383 (1998).
[22] Y. Q. Zhang *et al.,* Phys. Rev. Lett. **62**, 1848 (1989).
[23] J. Zheng, C. X. Yu, and Z. J. Zheng, Phys. Plasmas **4**, 2736 (1997).
[24] A. B. Langdon, Phys. Rev. Lett. **44**, 575 (1980).
[25] L. Spitzer, Jr. and R. Härm, Phys. Rev. **89**, 977 (1953).
[26] J. P. Matte *et al.,* Plasma Phys. Controlled Fusion **30**, 1665 (1988).
[27] G. B. Zimmerman and W. L. Kruer, Comments Plasma Phys. Controlled Fusion **2**, 85 (1975).
[28] B. G. Wilson *et al.,* in *Radiative Properties of Hot Dense Matter,* edited by W. Goldstein, C. Hooper, J. Gauthier, J. Seely, and R. Lee (World Scientific, Singapore, 1991).
[29] S. H. Glenzer *et al.,* Phys. Rev. Lett. **80**, 2845 (1998).